Hot-Star Winds: CIRs, DACs & BRITE Spots

Stanley P. Owocki[1]

1. Bartol Research Institute, Department of Physics and Astronomy, University of Delaware, Newark, DE 19716 USA

The high luminosities of massive stars drive strong stellar winds, through line scattering of the star's continuum radiation. After summarizing the basic, steady-state CAK theory for wind driving by a power-law ensemble of lines, the discussion here examines the origin of migrating *discrete absorption components* (DAC's) commonly seen in UV wind lines, with focus on the *bright spot* model proposed more than 20 years ago by Cranmer & Owocki. Within modern constraints of hot-star photometric variability observed by the BRITE satellites, we present a semi-analytic analysis for the spot size and amplitude needed to produce an overloaded wind that develops a kink transition to a slowly decelerating velocity plateau that form the DAC.

1 Introduction

UV spectra of hot, luminous stars show P-Cygni line profiles characteristic of a strong, high speed stellar wind outflow. Castor, Abbott & Klein (CAK; 1975) developed the basic steady-state theory for the driving of such winds via scattering of the star's UV continuum radiation by a large ensemble of spectral lines. Temporal monitoring (mainly from IUE) revealed that unsaturated P-Cygni lines commonly show "discrete absorption components" (DAC's) that migrate blueward from line-center over several days (Howarth & Prinja, 1989; Kaper et al., 1999), features not predicted in the steady-state CAK model. Arguing from analogy with the solar wind, Mullan (1986) proposed that unresolved structure near the stellar surface could, when coupled with the stellar rotation, produce spiral "co-rotating interaction regions" (CIR's) in the wind, with associated density compressions leading to the observed DAC's. Time-dependent, 2D radiation hydrodynamical simulations by Cranmer & Owocki (1996, hereafter CO96), showed that bright spots on the surface could increase the local mass flux, leading to an overloading that slowed the outflow, with CIR's then produced by the interaction with the ambient, faster wind. Synthetic UV spectra from these simulations did indeed produce DAC's with many of the observed features, but these were found to stem not from the density compressions, but rather from *velocity plateaus* that follow an abrupt "kink" transition from acceleration to coasting of the overloaded wind stream. Motivated by recent direct evidence for such bright spots in observations of hot stars by the BRITE satellites (Ramiaramanantsoa et al., 2018), the paper here develops a semi-analytic basis for determining the spot size and brightness needed to induce such kink transitions within the observational constraints of a typical 10 mmag variation in visual bands.

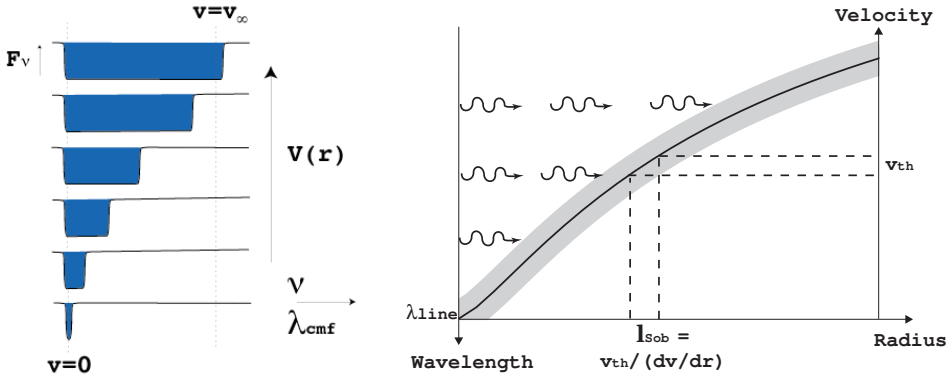

Fig. 1: Two perspectives for the Doppler-shifted line-resonance in an accelerating flow. Right: Photons with a wavelength just shortward of a line propagate freely from the stellar surface up to a layer where the wind outflow Doppler shifts the line into a resonance over a narrow width (represented here by the shading) equal to the Sobolev length, set by the ratio of thermal speed to velocity gradient, $l_{\rm Sob} \equiv v_{\rm th}/(dv/dr)$. Left: Seen from successively larger radii within the accelerating wind, the Doppler-shift sweeps out an increasingly broadened line absorption trough in the stellar spectrum.

2 Sobolev-based Models for Steady-State Line-Driven Stellar Winds

2.1 CAK Point-Star Model

As illustrated in Fig. 1, a key feature for line driving in an expanding wind is the desaturation of the lines by wind acceleration (shown in left panel), with photons initially at shorter wavelength from a line becoming Doppler-shifted (right panel) into resonance over a narrow layer of width by the ratio of the line thermal width to the local velocity gradient, $\ell_{\rm Sob} \equiv v_{\rm th}/(dv/dr)$, known as the Sobolev length (Sobolev, 1960). This Sobolev approximation allows the line-force to be written in terms of the *local* velocity gradient and density.

For line driving that overcomes gravity to yield a net acceleration $v(dv/dr)$ in the radial flow speed $v(r)$, we can write the equation of motion in dimensionless form in which all accelerations are scaled by the net effective gravity (after reduction by electron scattering),

$$w' = -1 + \tilde{\Gamma}_{\rm CAK}\,, \tag{1}$$

where $w \equiv v^2/v_{\rm esc}^2$ and $w' \equiv dw/dx$, with $x \equiv 1 - R_*/r$ and $v_{\rm esc} \equiv \sqrt{2GM_*(1-\Gamma_{\rm e})/R_*}$ is the effective escape speed from the stellar surface radius R_*. For a star of luminosity L_* and mass M_*, the effective gravity is reduced by the continuum force from free-electron scattering, set by Eddington factor $\Gamma_{\rm e} \equiv \kappa_{\rm e} L_*/GM_*c$ times the local stellar gravity GM_*/r^2 at radius r.

The *resonant* nature of line scattering means the associated radiative acceleration is generally much larger, up to a factor $\Gamma_{\rm thin}/\Gamma_{\rm e} = \bar{Q} \approx 2000(Z/Z_\odot)$ in the idealized optically thin limit that the lines are illuminated by unattenuated continuum flux, where $\bar{Q}$ represents a combination of the "quality" of the line resonances and the relative fraction of electrons bound into metal ions, and $Z/Z_\odot$ is the metallicity in solar units (Gayley, 1995). In the general case that some lines are optically thick

within the Sobolev resonance zone, the scaled CAK line acceleration takes the form,

$$\tilde{\Gamma}_{\rm CAK} = \frac{\overline{Q}\Gamma_{\rm e}}{(1-\alpha)(1-\Gamma_{\rm e})(\overline{Q}t)^\alpha} = C(w')^\alpha \,, \tag{2}$$

where $t \equiv \kappa_{\rm e}\rho c/(dv/dr)$, and $\alpha \approx 0.5 - 0.65$ is the CAK power-law index. The last equality relates the line-force to the flow acceleration, with

$$C \equiv \frac{1}{1-\alpha}\left[\frac{L_*}{\dot{M}c^2}\right]^\alpha \left[\frac{\overline{Q}\Gamma_{\rm e}}{1-\Gamma_{\rm e}}\right]^{1-\alpha} , \tag{3}$$

with $\dot{M} \equiv 4\pi\rho v r^2$ the mass loss rate. Note that, for fixed sets of parameters for the star (L_*, M_*, $\Gamma_{\rm e}$) and line-opacity (α, $\overline{Q}$), this constant scales with the mass loss rate as $C \propto 1/\dot{M}^\alpha$. Application of eqn. (2) into (1) gives the CAK equation of motion (EOM),

$$F = w' + 1 - C(w')^\alpha = 0 \,. \tag{4}$$

As illustrated in Fig. 2, for small $\dot{M}$ (large C), there are two solutions, while for large $\dot{M}$ (small C), there are no *accelerating* solutions, i.e., with $w' > 0$. The CAK critical solution corresponds to a *maximal* mass loss rate with purely accelerating solutions, defined by $\partial F/\partial w' = 0$, for which the $C(w')^\alpha$ is tangent to the line $1 - \Gamma_{\rm e} + w'$ at a critical acceleration $w'_c = (1-\Gamma_{\rm e})\alpha/(1-\alpha)$ (see solid line and curve in Fig. 2). Since the scaled equation of motion (4) has no explicit spatial dependence, this critical acceleration applies throughout the wind, and so can be trivially integrated to yield $w(x) = w'_c\, x$. In terms of dimensional quantities, this represents a specific case of the general "beta"-velocity-law,

$$v(r) = v_\infty \left(1 - \frac{R_*}{r}\right)^\beta , \tag{5}$$

where here $\beta = 1/2$, and the wind terminal speed $v_\infty/v_{\rm esc} = \sqrt{\alpha/(1-\alpha)} \approx 1 - 1.4$. Similarly, the critical value $C_{\rm c} = \alpha^{-\alpha}(1-\alpha)^{\alpha-1}$ yields, through eqn. (3), the standard CAK scaling for the mass loss rate

$$\dot{M}_{\rm CAK} = \frac{L_*}{c^2}\,\frac{\alpha}{1-\alpha}\left[\frac{\overline{Q}\Gamma_{\rm e}}{1-\Gamma_{\rm e}}\right]^{(1-\alpha)/\alpha} . \tag{6}$$

2.2 Corrections for Finite Stellar Disk and Variable Ionization

These classical CAK scalings strictly apply only under the idealized assumption that the stellar radiation is radially streaming from a point-source. For a star with a constant surface brightness, integration over the stellar disk leads to a finite-disk correction factor of the form (CAK eqn. 50),

$$f_{\rm d}(r) \equiv \frac{g_{\rm fd}}{g_{\rm CAK}} = \frac{(1+\sigma)^{1+\alpha} - (1+\sigma\mu_*^2)^{1+\alpha}}{(1+\alpha)\sigma(1+\sigma)^\alpha(1-\mu_*^2)} \,, \tag{7}$$

with $\mu_* \equiv \sqrt{1 - R_*^2/r^2}$ the cosine of the finite-cone angle of the stellar disk, and $\sigma \equiv d\ln v/d\ln r - 1$. The complex dependence on radius, velocity, and velocity gradient now precludes self-consistent analytic wind solutions, like those obtained above for

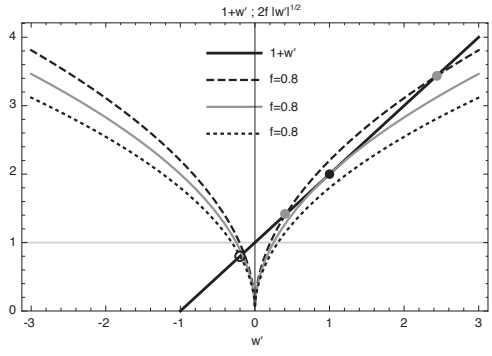

Fig. 2: "Seagull diagram" for graphic solutions between gravity and inertia (diagonal line for $1 + w'$) and a line-force that now scales with the square root of the *absolute value* of the scaled acceleration $\sqrt{|w'|}$. The intersection on the left wing gives decelerating solutions, with $w' < 0$ for the subcritical case $f < 0.8$.

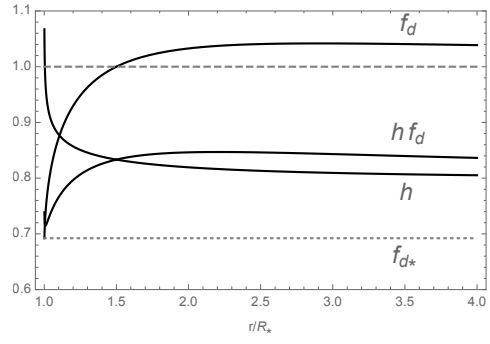

Fig. 3: Comparison of the radial variations of the finite-disk correction factor $f(r)$, the ionization correction factor $h(r)$ for $\delta = 0.1$, and their product $h(r)f(r)$, assuming a 'beta' velocity law $v(r) = v_\infty(1 - R_*/r)^\beta$, taking here $\beta = 1/2$.

the point-star case, but numerical solutions have been derived independently by Friend & Abbott (1986) and Pauldrach et al. (1986).

A key result is that near the stellar surface the radiative force is reduced by a factor $f_{\rm d*} \approx 1/(1+\alpha)$, leading to a reduced mass loss rate

$$\dot{M}_{\rm fd} = f_{\rm d*}^{1/\alpha}\dot{M}_{\rm CAK} = \frac{\dot{M}_{\rm CAK}}{(1+\alpha)^{1/\alpha}} \approx \dot{M}_{\rm CAK}/2\,. \tag{8}$$

Away from the star, the correction factor increases back toward unity, which for the reduced base mass flux implies a stronger, more extended acceleration, giving a somewhat higher terminal speed, $v_\infty \approx 3v_{\rm esc}$, and a flatter velocity law, approximated by replacing the exponent in eqn. (5) by $\beta \approx 0.8$.

Another simplifying assumption of the original CAK analysis was that the line-opacities are spatially constant, with a fixed wind ionization. Abbott (1982) showed that the effect of a radial change in ionization can be approximately taken into account by correcting the CAK force (2) by a factor of the form

$$h(r) = \left(\frac{n_{\rm e}}{W\,10^{11}}\right)^{\delta}, \tag{9}$$

where $n_{\rm e}$ is the electron number density in cm^{-3}, $W \equiv 0.5(1 - \sqrt{1 - R_*/r})$ is the radiation "dilution factor", and the exponent has a typical value $\delta \approx 0.1$. This factor introduces an additional density dependence to that already implied by the optical depth factor $1/t^\alpha$ given in eqn. (2). Its overall effect can be roughly accounted with the simple substitution $\alpha \to \alpha' \equiv \alpha - \delta$ in the power exponents of the CAK mass loss scaling law (6). The general tendency is to moderately increase $\dot{M}$, and accordingly to somewhat decrease the wind speed. For $\delta = 0.1$, Fig. 3 plots the radial variation of these finite-disk and ionization correction factor for a simple $\beta = 1/2$ velocity

law, with a mass loss rate that gives a fiducial $n_e = 10^{11}\mathrm{cm}^{-3}$ at a location where $v = v_\infty/10$.

3 The Bright-Spot Model for Discrete Absorption Components

3.1 Conditions for Kink Transitions: the "Seagull Diagram"

In the context of this conference's focus on the BRITE satellites, let us now review some basic theoretical issues behind modeling DACs within the CO96 "Bright Spot" (BS) paradigm. As noted, the DAC's that arise in this BS model do *not* form from the enhanced density of the compression co-rotating interaction regions (CIR's), as envisioned in the original Mullan (1986) model for DAC's. Instead they stem from the extended *velocity plateaus* that form ahead of those dense compressions, after an abrupt "kink" in the velocity gradient that transforms the strong outward acceleration into a rather slow deceleration or "coasting" region that is the basis of the plateau.

The basis for kink solutions lies in the velocity gradient dependence of the CAK line force. For more realistic cases than the simple CAK point-star model, the constant C in the EOM (4) can be multiplied by a correction function $f(r)$ that accounts for additional effects, e.g. due to the finite-disk (f_d) of the star, variations in ionization (h), or indeed spots (f_s) of variable brightness. For the simple $\alpha = 1/2$ case, we can rewrite the EOM (4) in the form

$$F = 1 + w' - 2f\sqrt{|w'|} = 0\,, \tag{10}$$

where we have normalized the total correction factor such that $f = 1$ corresponds to the standard critical case, and the absolute values here reflect that the Sobolev model for local line absorption applies in principle to both positive and negative velocity gradients. As illustrated in Fig. 2, the CAK force terms with $\sqrt{|w'|}$ now has a left/right $(-/+)$ symmetric variation about $w' = 0$, giving the appearance reminiscent of the flapping wings of a bird, like a Seagull. The height of the wings depends on the factor f, with the dotted, solid, and dashed curves set by $f = 0.8$, 1, and 1.2. The black dot represents the CAK critical solution, while the gray dots represents the weak and strong positive accelerations that arise from a local increase in the line driving.

The dotted curve, which is the line-force with a 20% reduction below the critical value, no longer has any solution with positive acceleration; but it does now still have a back-up, slowly decelerating solutions with $w' < 0$, as denoted by the open black circle. Roughly speaking, the Sobolev line transfer that gave $\Gamma_\mathrm{CAK} \sim w'^\alpha$ also works approximately (i.e. within some caveats regarding multiple resonance points) for $w' < 0$ if we just assume $\Gamma_\mathrm{CAK} \sim |w'|^\alpha$. If a wind initially has $f > 1$ and thus positive acceleration $w' > 0$, but then has a reduction to $f < 1$, for which there are no longer solutions with $w' > 0$, it just switches to a *decelerating* case, $w' < 0$, thus leading to a kink in the wind velocity law.

3.2 Bright Spot Flux Enhancement

Such kinks thus arise whenever the net driving efficiency factor f declines outward to less than unity; they appear, for example, in the X-ionization "shadow wind" of

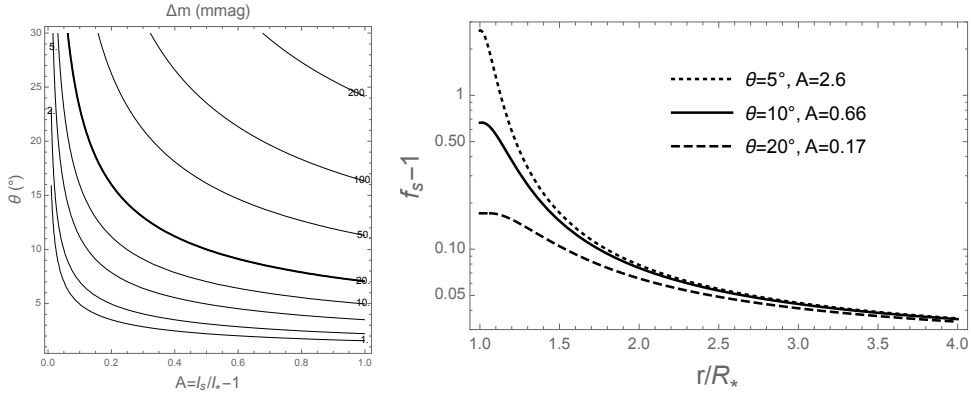

Fig. 4: Left: Contours of photometric variation (in mmag) plotted vs. spot angular size (θ) and amplitude A. Right: Radial variation of spot enhancement of the line-driving force for various combinations of spot size θ and amplitude A that give a UV photometric variability of 20 mmag.

high-mass X-ray binaries, and in the outer regions of winds from rapidly rotating stars (Madura et al., 2007). For localized bright spots, the initial driving is enhanced near the surface, inducing a locally enhanced mass flux. But as the solid angle of the spot drops with increasing distance, the enhancement sharply declines, leading to a possible overloading beyond what the local driving can sustain, and so a kink switch to a decelerating solution. To illustrate this semi-quantitatively, let us write a simple scaling relation for the local enhancement $f_{\rm s}(r)$ in the radiative flux at some radius r above a uniformly bright spot with angular radius θ and differential brightness enhancement A ($= I_{\rm s}/I_* - 1$). Using units in which the star has unit radius $R_* = 1$, this is given by

$$f_{\rm s}(r) = 1 + \frac{A r^2 \sin^2\theta}{1 + r^2 - 2r\cos\theta} \quad ; \quad r > \frac{1}{\cos\theta}\,. \tag{11}$$

For near-star radii $r \le 1/\cos\theta$, the spot fills the full disk and so the enhancement is just the constant factor $f_{\rm s} = 1 + A$. At very large distances $r \to \infty$, the observed flux is enhanced by a factor $f_{\rm s}(\infty) = 1 + A\sin^2\theta$, corresponding to an observed magnitude change $\Delta m = 2.5\log(1 + A\sin^2\theta)$.

Observations by the MOST and BRITE space observatories typically show O-star photometric variations of about one percent, or 10 mmag (Ramiaramanantsoa et al., 2014, 2018), in the visible. For hot stars, the temperature variation for such 1% variation in the visible would give about twice the amplitude in the UV region responsible for most of the line-driving (David-Uraz et al., 2017). If we thus adopt 20 mmag variation for the UV driving flux, then for any given spot angular radius beta, we can write an associated upper limit to the brightness amplitude, $A_{\rm max} = 0.02/\sin^2\theta$. The left panel of Fig. 4 shows a contour plot of this magnitude change (in mmag) as one varies θ and A, while the right panel plots $f_{\rm s}(r) - 1$ vs. r for various size spot models with this 10 mmag value for observed brightness variation.

Note that the smallest spots have the strongest base enhancements. They are thus better suited to overcoming the general outward increase from the finite-disk correction, which represents a kind of "safety factor" for maintaining a positive out-

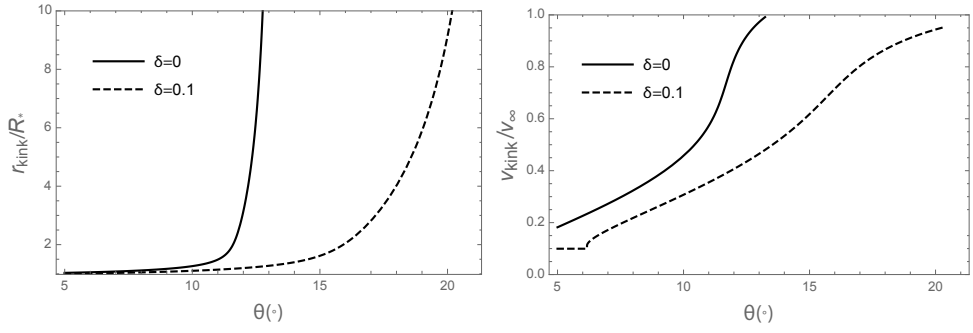

Fig. 5: Left: Kink radius $r_{\rm kink}$ as a function of spot size for spots giving 20 mmag UV photometric variation, for case with no ionization correction ($\delta = 0$), and with $\delta = 0.1$ Right: Associated velocity of the kink for a $\beta = 1/2$ velocity law prior to the kink.

ward acceleration. But since DACs are sometimes observed to nearly saturate to black, their associated structure must sometimes cover the entire stellar disk. At any local wind radius r, the wind structure induced by a spot of angular radius θ has a local radius $R_{\rm s} = \theta r$, which to cover the stellar disk must be bigger than the stellar radius R_*. For a wind radius $r/R_* \approx 2 - 3$ this requires a quite large spot, $\theta \geq R_*/r = 0.3 - 0.5\,{\rm radian} \approx 20 - 30°$. The 2% inferred upper limit on UV brightness variations requires quite small brightness variations for such large spots, i.e. $A < 0.1$.

Thus a general issue for BS models is keeping the brightness variation within the observed limit but having a spot size big enough to produce structures that can cover the disk to produce saturated DACs. At the same time, the spot amplitude must be strong enough that the initial increase of mass loss in the spot overloads the wind to level that can overcome the finite-disk safety factor. For a given spot model, we can define a total net, surface normalized force factor $f \equiv f_{\rm s}\, f_{\rm d}\, h/(f_{\rm s*} f_{\rm d*}\, h_*)$. Solving for the location where this falls back to the critical value $f = 1$ then gives the radius $r_{\rm kink}$ for a kink transition from accelerating to decelerating flow, with the associated kink velocity $v(r_{\rm kink})$ giving the onset of a discrete absorption component in the line profile.

Fig. 5 plots the variations of this kink radius (left) and kink velocity (right) as a function of spot angular size θ for spot amplitudes that give the canonical 20 mmag UV photometric variability. Note that including an ionization correction with exponent $\delta = 0.1$ allows kinks to form from larger, less bright spots than a standard model without ionization correction ($\delta = 0$). This reflects the ionization reduction in the finite-disk safety factor, which makes the overloading from spots more effective in inducing kink transitions to decelerating solutions.

The net upshot here is that the ionization correction term, which was not included in the original CO96 BS simulations, can reduce the finite-disk safety factor, and so could help make it possible to produce kinks and plateaus over a relatively large area of the stellar disk, with moderately large spots ($\theta \sim 10°$) with modest brightness enhancements, $A \approx 0.3$. David-Uraz et al. (2017) recently carried out hydrodynamical simulations of CIR and DAC formation for spots of various sizes, and with and without an ionization factor. While the results do show some depen-

dency on ionization correction, the effect is not as distinctive as suggested by the scaling analysis here. In addition, as discussed by Madura et al. (2007), in rapidly rotating stars the centrifugal acceleration increases the base mass flux and so can assist or cause an overloading that leads to kinks. Future work is needed to clarify the physical basis for these effects, and to more completely explore the efficacy of the BS model for reproducing the properties of observed DACs.

Acknowledgements. I acknowledge support via sabbatical leave from the University of Delaware. I thank A. David-Uraz, V. Petit, J. Sundqvist and G. Wade for helpful discussions on various topics discussed in this article. The concepts behind the seagull diagram originated from discussions with K. Gayley.

References

Castor, J. I., Abbott, D. C., Klein, R. I., *ApJ* **195**, 157 (1975)

Cranmer, S. R., Owocki, S. P., *ApJ* **462**, 469 (1996), arXiv: astro-ph/9508004

David-Uraz, A., et al., *MNRAS* **470**, 3672 (2017), arXiv: 1706.03647

Friend, D. B., Abbott, D. C., *ApJ* **311**, 701 (1986)

Gayley, K. G., *ApJ* **454**, 410 (1995)

Howarth, I. D., Prinja, R. K., *ApJS* **69**, 527 (1989)

Kaper, L., Henrichs, H. F., Nichols, J. S., Telting, J. H., *A&A* **344**, 231 (1999), arXiv: astro-ph/9812427

Madura, T. I., Owocki, S. P., Feldmeier, A., *ApJ* **660**, 687 (2007), arXiv: astro-ph/0702007

Mullan, D. J., *A&A* **165**, 157 (1986)

Pauldrach, A., Puls, J., Kudritzki, R. P., *A&A* **164**, 86 (1986)

Ramiaramanantsoa, T., et al., *MNRAS* **441**, 910 (2014), arXiv: 1403.7843

Ramiaramanantsoa, T., et al., *MNRAS* **473**, 5532 (2018), arXiv: 1710.08414

Sobolev, V. V., Moving envelopes of stars, Cambridge: Harvard University Press (1960)

Stan Owocki, Matt Shultz, Thomas Kallinger and Alexandre David-Uraz giving their talks.